Geochemistry Geophysics Geosystems G3
AN ELECTRONIC JOURNAL OF THE EARTH SCIENCES
Published by AGU and the Geochemical Society

Technical Brief
Volume 9, Number 7
25 July 2008
Q07021, doi:10.1029/2008GC001949
ISSN: 1525-2027

Click Here for Full Article

Resolution of direction of oceanic magnetic lineations by the sixth-generation lithospheric magnetic field model from CHAMP satellite magnetic measurements

S. Maus
CIRES, University of Colorado, Boulder, Colorado, USA

National Geophysical Data Center, NOAA, NOAA E/GC1, 325 Broadway, Boulder, Colorado 80305-3328, USA (stefan.maus@noaa.gov)

F. Yin and H. Lühr
GeoForschungsZentrum Potsdam, Telegrafenberg, Potsdam D-14473, Germany

C. Manoj
CIRES, University of Colorado, Boulder, Colorado, USA

National Geophysical Data Center, NOAA, NOAA E/GC1, 325 Broadway, Boulder, Colorado 80305-3328, USA

M. Rother, J. Rauberg, I. Michaelis, and C. Stolle
GeoForschungsZentrum Potsdam, Telegrafenberg, Potsdam D-14473, Germany

R. D. Müller
School of Geosciences, University of Sydney, Sydney, New South Wales 2006, Australia

[1] The CHAMP satellite continues to provide highly accurate magnetic field measurements from decreasing orbital altitudes (<350 km) at solar minimum conditions. Using the latest 4 years (2004–2007) of readings from the CHAMP fluxgate magnetometer, including an improved scalar data product, we have estimated the lithospheric magnetic field to spherical harmonic degree 120, corresponding to 333 km wavelength resolution. The data were found to be sensitive to crustal field variations up to degree 150 (down to 266 km wavelength), but a clean separation of the lithospheric signal from ionospheric and magnetospheric noise sources was achieved only to degree 120. This new MF6 model is the first satellite-based magnetic model to resolve the direction of oceanic magnetic lineations, revealing the age structure of oceanic crust.

Components: 4040 words, 8 figures.

Keywords: lithospheric field; crustal field; satellite geomagnetism; ocean spreading anomalies; magnetic anomalies.

Index Terms: 1541 Geomagnetism and Paleomagnetism: Satellite magnetics: main field, crustal field, external field; 1545 Geomagnetism and Paleomagnetism: Spatial variations: all harmonics and anomalies; 1550 Geomagnetism and Paleomagnetism: Spatial variations attributed to seafloor spreading (3005).

Copyright 2008 by the American Geophysical Union

Received 17 January 2008; **Revised** 14 May 2008; **Accepted** 25 June 2008; **Published** 25 July 2008.

Maus, S., F. Yin, H. Lühr, C. Manoj, M. Rother, J. Rauberg, I. Michaelis, C. Stolle, and R. D. Müller (2008), Resolution of direction of oceanic magnetic lineations by the sixth-generation lithospheric magnetic field model from CHAMP satellite magnetic measurements, *Geochem. Geophys. Geosyst.*, *9*, Q07021, doi:10.1029/2008GC001949.

1. Introduction

[2] Satellites in low-Earth orbit (LEO) provide the most effective means of mapping the long wavelengths of the magnetic field caused by the magnetization of the Earth's lithosphere. A comprehensive overview of satellite lithospheric magnetic field modeling was given by *Langel and Hinze* [1998]. Initial satellite magnetic anomaly maps were produced from POGO data [*Regan et al.*, 1975]. In 1979–1980, Magsat was the first satellite to carry an accurate vector magnetometer with attitude determination from a star tracker [*Cain et al.*, 1989; *Arkani-Hamed et al.*, 1994; *Ravat et al.*, 1995]. Substantial progress was made with the CHAMP satellite, launched in July 2000. Apart from an order of magnitude improvement in magnetometer accuracy, CHAMP was designed to remain in LEO for many years, leading to excellent spatial and temporal data coverage. A high inclination of 87.3° minimizes the polar gap. Here, we describe the sixth generation of the MF series of CHAMP lithospheric magnetic field models [*Maus et al.*, 2002, 2006, 2007a]. Our new model MF6 extends to spherical harmonic degree 120, corresponding to a resolution of 333 km wavelength. For the first time, the oceanic magnetic lineations have become visible on a global scale, providing valuable information on the age structure and evolution of the oceanic crust.

2. Data Selection and Processing

[3] In the data selection and processing sequence, we closely followed the procedures used in the previous MF4 [*Maus et al.*, 2006] and MF5 [*Maus et al.*, 2007a] models. The only significant changes were (1) the use of an improved scalar data product, (2) the decision not to correct for night side F region currents, (3) the use of B_Z as the only vector component data, and (4) the expansion to a higher spherical harmonic degree, enabled by the cleaner input data and the lower altitude of the CHAMP satellite. Finally, we investigated some alternative processing schemes.

2.1. CHAMP Data

[4] Two types of data are used for high-degree lithospheric field modeling: Vector component data and scalar $|B|$ data. Owing to uncertainties in the satellite attitude, vector component data have much higher noise levels than scalar measurements of the total field strength. Unfortunately, the scalar measurements do not completely determine an internal poloidal field [*Backus*, 1970]. Including vector component data is therefore unavoidable. The CHAMP satellite has two fluxgate vector magnetometers (FGM) and an absolute scalar Overhauser magnetometer (OVM). Fluxgate magnetometers experience drifts with time. Therefore, the scalar magnetometer is used for an absolute calibration of the vector magnetometer. After this calibration, it is advantageous to use the absolute field strength from the FGM vector magnetometer, rather than the readings of the scalar OVM magnetometer. The reason is that the FGM has a noise level of only 0.01 nT, compared to about 0.1 nT for the OVM. For high-degree field modeling a new 1 Hz scalar data product was therefore produced from a combination of the calibrated 50 Hz FGM readings and the OVM measurements. Short-period variations, up to about 1000s, were derived from the FGM and longer period signal from the stable OVM. This improved scalar data product was used here in combination with the usual vector component FGM readings.

[5] Data were selected for the period of January 2004 to September 2007. To avoid the influence of F region currents, which are strongest in the hours after sunset, only data from 22:00 to 05:00 local time were used. Further data selection criteria were Kp $\leq$1+ and, for high latitudes, a merging electric field at the magnetopause smaller than 0.8 mV/m, as recommended by *Ritter and Lühr* [2006]. We further discarded all tracks which were identified as being contaminated by magnetic signals because of plasma irregularities in the low-latitude ionosphere [*Stolle et al.*, 2006]. Vector data were used only for periods in which the star camera was operating in dual-head mode.

[6] Middle and high-latitude data were processed separately in order to account for the difference in

the properties of data collection in these regions. High-latitude tracks were defined as covering the regions poleward of |55°|, and middle-latitude tracks covering the overlapping range of −65° to 65° in magnetic latitude. The RMS of the residuals against POMME-4.0 (http://geomag.org/models/pomme4.html) for each track were then plotted as a function of longitude in order to identify and discard remaining tracks with abnormally high noise level.

2.2. Residual Computation

[7] In the first step, the main field to degree 15 and a simple magnetospheric model given by POMME-4.0 were subtracted. Furthermore, we subtracted the ocean tidal magnetic signal for the 8 dominant modes, using a prediction of *Kuvshinov and Olsen* [2005]. For MF5 we had also subtracted first-order predictions of gravity and pressure-driven F region currents. In the mean-time, we found that these corrections have serious shortcomings. In particular, they do not take into account that the westward electric field on the night-side partly inhibits the gravity-driven current. For MF6 we therefore decided not to apply any corrections for F region currents. This is justified (1) by the low solar flux level during the considered years and (2) by the omission of data from the early post-sunset hours.

2.3. Along-Track Filtering

[8] Remaining systematic offsets between neighboring tracks are mostly due to unmodeled contributions from magnetospheric currents, in particular the ring current, and from their induction [*Maus et al.*, 2002, Figure 2]. Being predominantly of long wavelength, this noise can be removed to a large extent by fitting and subtracting a degree-1 model on a track-by-track basis. We used the same filter parameters as in the processing for the MF5 model. For vector data, this included 3 external and 3 internal field parameters, plus a set of 3 angles accounting for the uncertainty in the satellite attitude. For scalar data, we co-estimated 2 components of an external dipole and one induced internal dipole coefficient. At mid latitudes we further corrected for the far-field effect of the auroral electrojet by means of a suitable model, as described in *Maus et al.* [2007a].

2.4. Line Leveling

[9] Even after filtering, significant non-lithospheric contributions lead to arbitrary offsets between adjacent tracks. These offsets can be reduced by minimizing the difference between neighboring tracks, and the difference at crossover points between ascending and descending tracks. Our line-leveling algorithm minimizes the distance-weighted misfit of the residuals against MF5 [*Maus et al.*, 2007a], between all nearest pairs of measurements for all pairs of tracks. To account for stronger variation in the vertical direction, vertical distances are up-weighted. The exact weight function is given by *Maus et al.* [2006].

[10] As for MF4 and MF5, the scalar data sets from the three latitude ranges (North Pole, South Pole and middle latitudes) were first leveled against each other using corrections up to spherical harmonic degree 20. Then the vector data were leveled onto the scalar data using corrections up to spherical harmonic degree 12.

2.5. Regularized Least Squares Estimation of Gauss Coefficients

[11] The estimation of the Gauss coefficients followed the procedure used for MF5. However, for the vector data, only the B_Z component was used. As suggested by *Lesur et al.* [2008], this helps to reduce contamination by unmodeled magnetospheric fields, which primarily affect the horizontal components. Also, the vector data were down-weighted by a factor 100 to account for their high noise levels. To avoid ringing at the poles, the polar gap was filled in with values from MF5. In the regularization scheme, described in detail by *Maus et al.* [2006], the empirical power model was revised to

$$R_0(\ell, m) = [0.1 + 0.35(1 - (m/\ell))^2](1 - 0.004(\ell - 81)) \quad (1)$$

accounting for a decrease in the crustal field power toward higher degrees. As in the inversion for MF5, regularization was applied only to coefficients above degree 80. To investigate the high-degree information content of the data, an initial model MF6-0 was estimated to degree 150. After visual inspection of the corresponding B_Z maps at geoid level, which indicated high-degree artifacts in some regions, the final MF6 model was expanded only to degree 120.

2.6. Recovery of Signal Lost by Filtering

[12] It has been recognized for some time that unfiltered field models, such as CM4 [*Sabaka et al.*, 2004], GRIMM [*Lesur et al.*, 2008], CHAOS [*Olsen et al.*, 2006] and POMME-4 (http://geomag.org/models/pomme4.html) have higher power levels than the MF series of models. Obviously, the along-

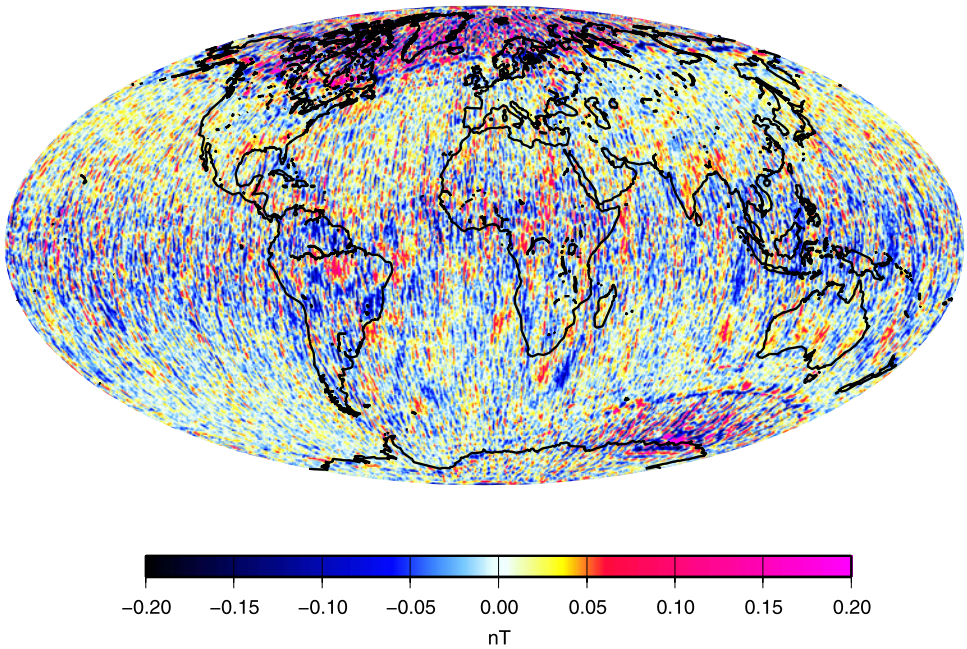

Figure 1. Residuals of the scalar data after subtracting the MF6-0 model to degree 150. The RMS of the residuals is 0.09 nT, which is only slightly higher than the fluxgate magnetometer instrument noise level of about 0.01 nT.

track filtering in the MF modeling procedure removes some genuine lithospheric signal. On the other hand, it has so far not been possible to recover coefficients beyond degree 65 from unfiltered data. R. Holme (personal communication, 2007) therefore suggested accounting for the effect of the filter by filtering not only the data, but also the Green's functions of the spherical harmonic coefficients for every track when assembling the normal equations matrix. Indeed, we implemented this suggestion and found that it works well, as long as the input data are not modified by line leveling. However, line-leveling constitutes an essential step in retrieving high-degree coefficients. We found that a model estimated by this procedure from filtered, but not line-leveled, data could be extended only up to a similar degree as a model from unfiltered data. Consequently, the recovery of genuine signal lost in filtering is difficult to implement. It was therefore decided to take the lower-degree coefficients from the (unfiltered) POMME-4 model and estimate the high-degree coefficients from filtered and line-leveled data.

3. Results

[13] A preliminary model MF6-0 was estimated to degree 150. The quality of this model was analyzed by inspecting the data residuals and its spectrum and degree-correlation with other models. Furthermore, maps of the vertical component of the field at the Earth's surface were examined for artifacts, and the trend direction of oceanic anomalies was compared with the isochrons of an oceanic age model.

3.1. Data Residuals

[14] Interestingly, the scalar and vector data do not agree equally well with the derived model. This can be seen when subtracting the MF6-0 model from the original data that went into the analysis. Figures 1 and 2show the residuals of the scalar and the B_Z data against the MF6-0 model. Since the scalar data were upweighted by a factor 100 over the B_Z data in the inversion, it is not surprising that the model fits the scalar data better than the B_Z data. Nevertheless, it is interesting that a model which fits the scalar data to an RMS of 0.09 nT, leaves residuals with an RMS of 1.1 nT in the B_Z data. This may partly be due to the stronger contamination of vector data by ionospheric currents. Also, the B_Z component data are affected by attitude uncertainties. Finally, the different filters and the different line-leveling are likely to create small inconsistencies between the two types of data. In general, we place higher trust in the scalar data, which were therefore more closely fitted in the modeling.

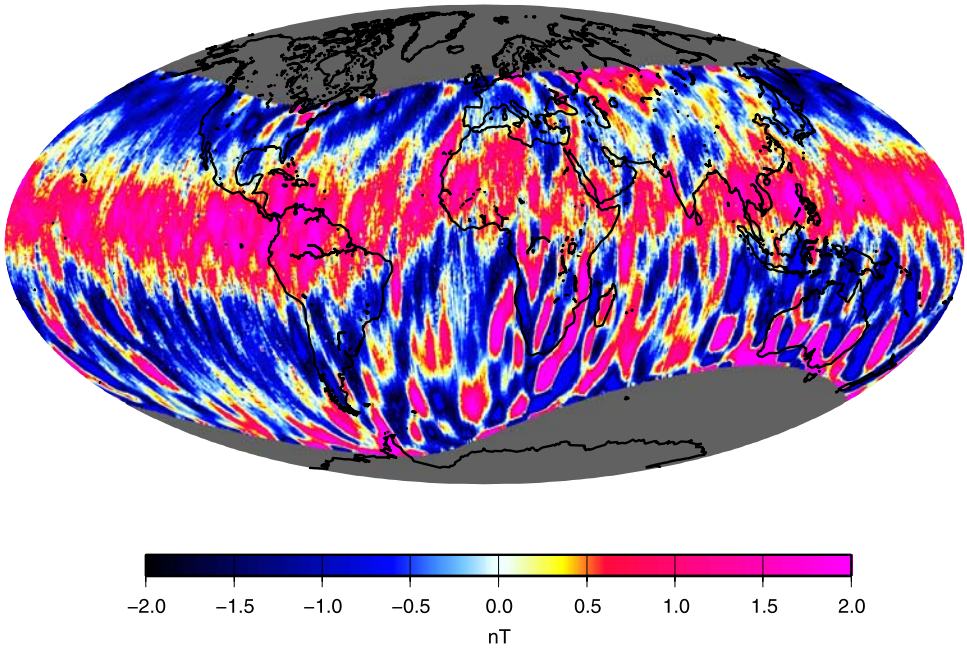

Figure 2. Residuals of the B_Z vector component data after subtracting the MF6-0 model to degree 150. Owing to the low weight assigned to the vector data in the inversion, inconsistencies between scalar and vector data are predominantly reflected in the vector residuals, which have an RMS of 1.1 nT.

3.2. Long Wavelengths

[15] A comparison of the MF6-0 spectrum with the spectra of models from unfiltered data is given in Figure 3. The MF6-0 spectrum is consistently weaker, which is partly a negative consequence of genuine signal loss in the filtering, and partly a positive consequence of lower noise levels. Presumably, the former effect dominates at lower degrees, while the latter effect dominates at higher degrees.

[16] To further investigate the respective roles of signal loss and noise contamination, we display in Figure 4 the degree correlation, as defined in equation (4.23) of *Langel and Hinze* [1998], between all pairs of the models GRIMM, POMME-4, and MF6-0. At degrees less than 45, the correlation between the unfiltered models GRIMM and POMME-4 is significantly higher than the correlation between either of these models and MF6-0. This can be considered as evidence that the signal loss due to filtering is the dominant effect at these lower degrees. At degree 45, however, the correlation curves cross over, and at higher degrees the correlation between GRIMM and POMME-4 is lower than the correlation between either of these models and MF6-0. This indicates that for degrees beyond 45 the noise contamination of the unfiltered models is higher than the loss of genuine signal through filtering. This interpretation is also supported by the spectral curves in Figure 3, which significantly diverge above degree 50.

3.3. Short Wavelengths

[17] A verification of the high-degree part of the model can be gained from a comparison with independent marine and aeromagnetic data. In producing the NGDC World Magnetic Anomaly Map [*Maus et al.*, 2007b], we merged all of the near-surface data. To our knowledge, none of these data incorporated any long wavelength satellite-derived information. From the near-surface grid of total intensity anomaly data, we estimated a spherical harmonic model to degree 150. The Backus effect was avoided by setting the coefficients with $m = \pm\ell$ to zero, and by further eliminating eigenvectors with small eigenvalues.

[18] Figure 5 shows a comparison of the POMME-4 and MF6-0 spectra with the spectrum of the marine and aeromagnetic grid. The latter is contaminated at long wavelengths by incompletely removed main fields and spurious features introduced in stitching together individual small-scale survey patches. At short wavelengths, however, the spectrum of the near-surface is consistent with the satellite derived models. The degree correlation (Figure 6) is consistently higher than 0.5 up to

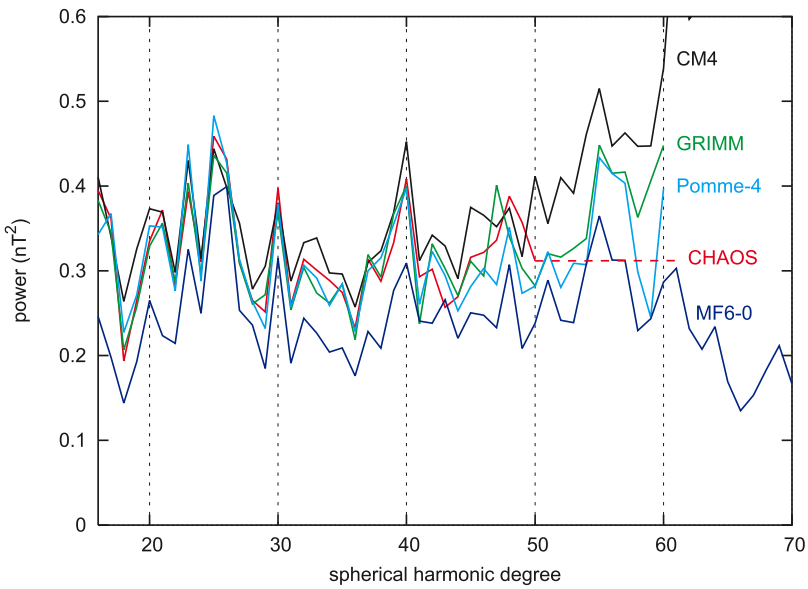

Figure 3. Power spectra of the CM4 [*Sabaka et al.*, 2004], GRIMM [*Lesur et al.*, 2008], POMME-4 (http://geomag.org/models/pomme4.html), and CHAOS [*Olsen et al.*, 2006] models from unfiltered data, compared with MF6-0 from filtered data. The CHAOS model extends only to degree 50.

degree 120, and then gradually drops to zero at degree 150.

3.4. Synthesis of the Final MF6 Model

[19] Judging from the spectrum and degree correlation in Figures 5 and 6, one could justify expanding MF6 up to degree 140. However, visual inspection of the corresponding maps of the field at the Earth's surface reveals spurious small-scale north-south trending stripes in some areas of weak lithospheric signal. We therefore take a conservative approach and truncate the final MF6 model at degree 120. Similar visual inspection of the POMME-4 model indicates that it is clean up to degree 54. We therefore take the coefficients of degree 16–54 from the POMME-4 model and

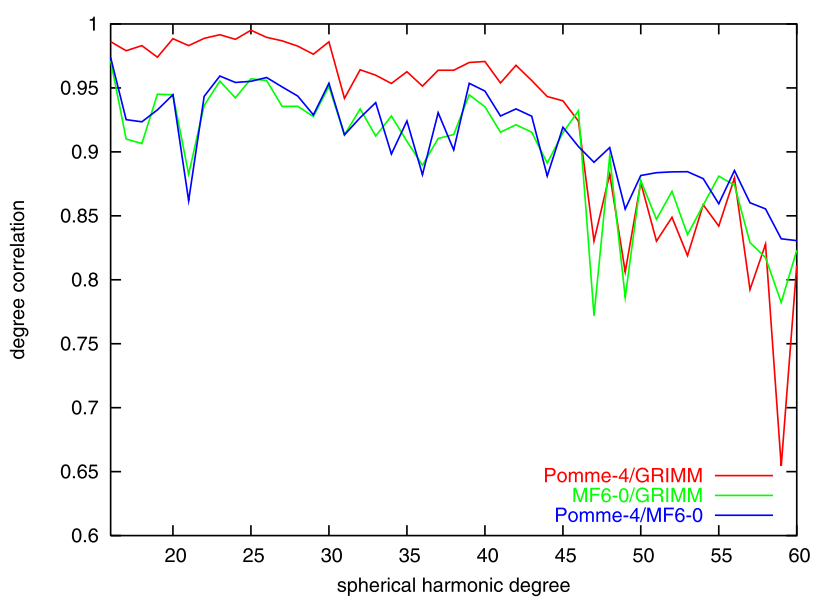

Figure 4. Degree correlation between all pairs of the models GRIMM, POMME-4, and MF6-0. The crossover at degree 45 can be interpreted as the degree above which the benefit of filtering outweighs the drawback of losing genuine signal.

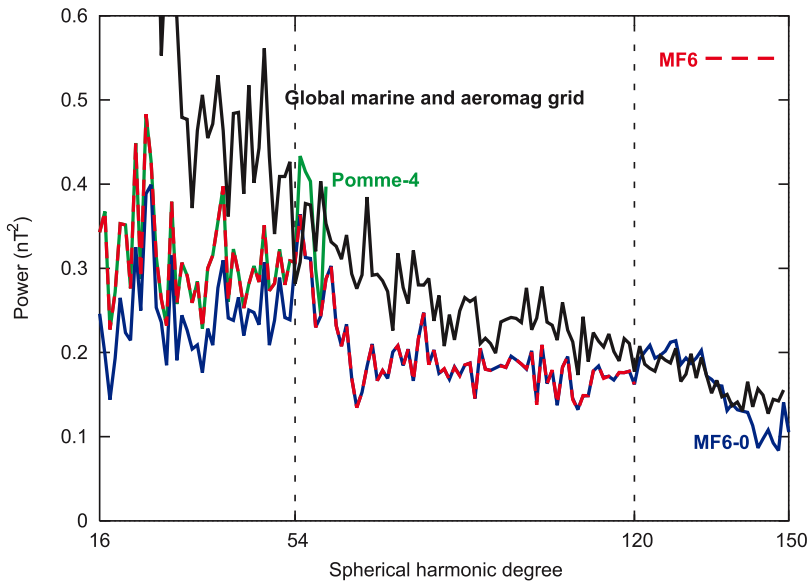

Figure 5. Power spectra of POMME-4 and MF6-0 compared with the spectrum of a grid compiled from marine and aeromagnetic data. The final MF6 model is synthesized by combining degrees 16–54 of POMME-4 with degrees 55–120 of MF6-0.

merge them with the coefficients of degrees 55–120 of MF6-0 for the final MF6 model. The spectrum of the MF6 model is indicated as a dashed line in Figure 5.

3.5. Comparison With Age of the Oceanic Crust

[20] Oceanic crust is formed at the spreading centers of mid-ocean ridges. When newly formed crust cools to below the Curie temperature of titano-magnetite, it acquires a remanent magnetization parallel to the ambient geomagnetic field. Polarity reversals of the geomagnetic field then lead to magnetization features which are parallel to the isochrons (lines of equal age) of the oceanic crust.

[21] Figure 7 shows the vertical component of the MF6 magnetic field at the Earth's surface. Overlain

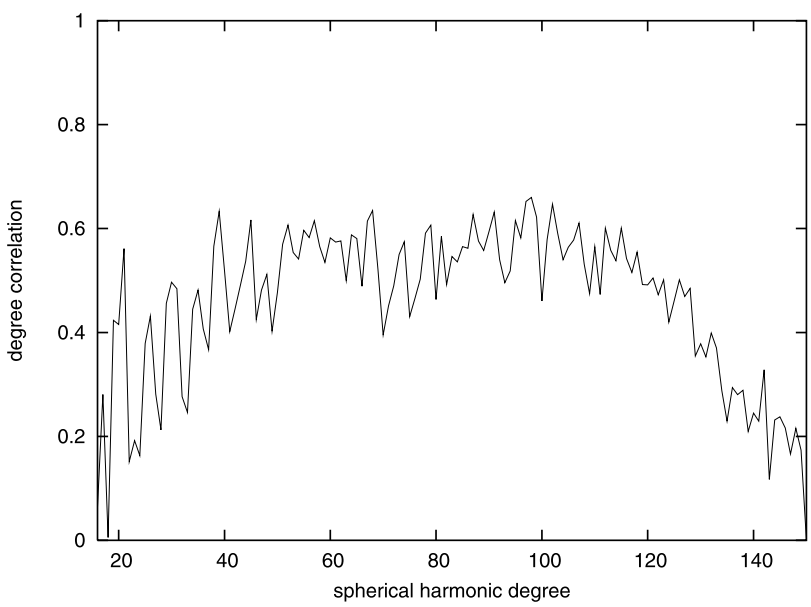

Figure 6. Degree correlation between MF6-0 and the independent model estimated from marine and aeromagnetic data. The correlation starts to decrease at degree 120, which is chosen as the cutoff for the final model, MF6.

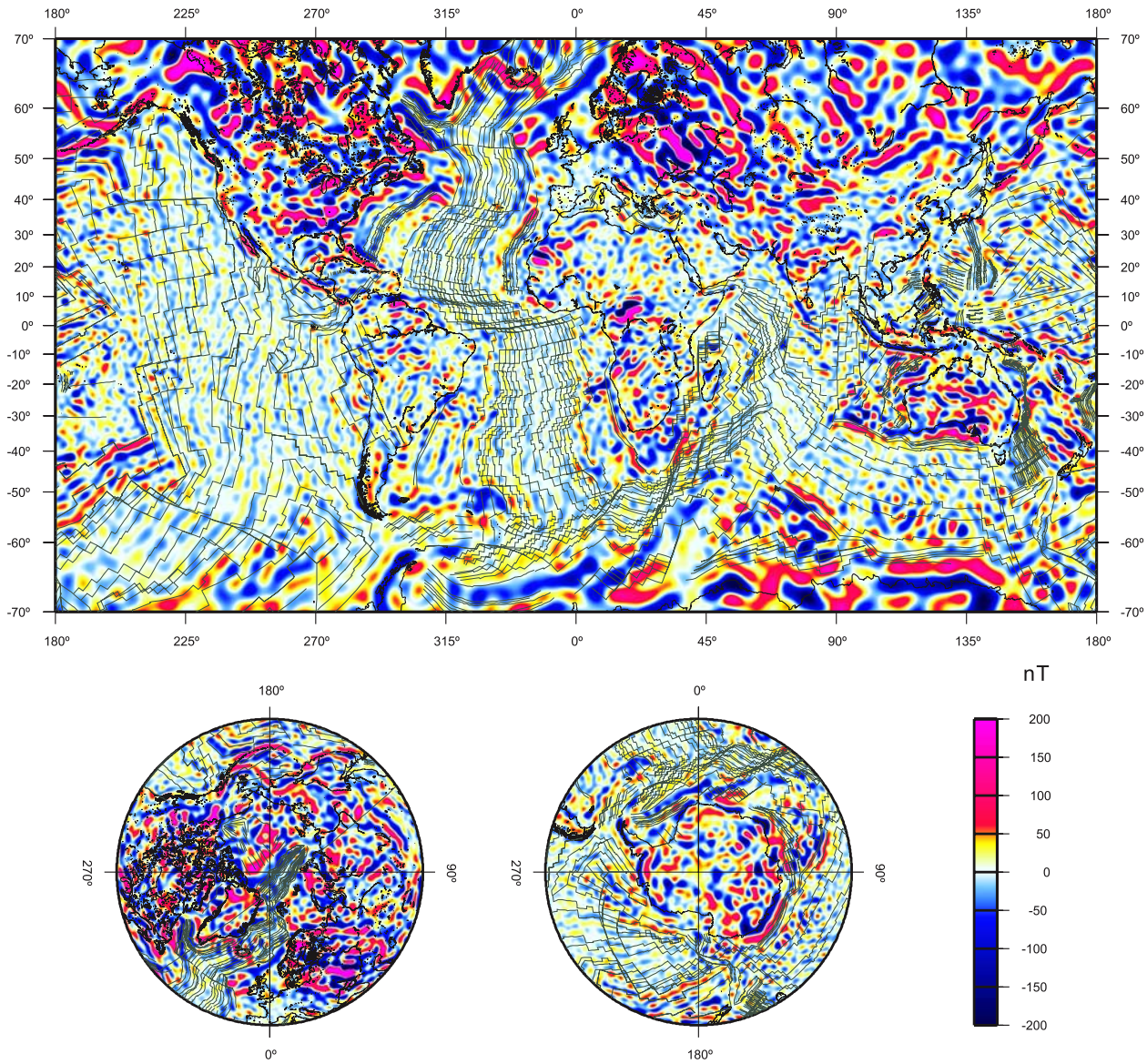

Figure 7. Vertical component of the lithospheric magnetic field at the Earth's surface overlain with the isochrons of an ocean-age model inferred from independent marine and aeromagnetic data by *Müller et al.* [2008].

in dark green are the isochrons of the new oceanic crustal age model of *Müller et al.* [2008]. In most regions we find excellent agreement between the trend of the oceanic magnetic anomalies and the isochrons.

[22] This interpretation is further supported by a statistical analysis: If the oceanic magnetic anomalies predominantly follow the isochrons, then it is to be expected that the anomalies exhibit smaller variations parallel than perpendicular to the isochrons of the oceanic crustal age model. We verified this behavior by estimating the 2-D autocorrelation function (ACF)

$$\mathrm{ACF}(\boldsymbol{\tau}) = \langle B_z(\mathbf{r}) B_z(\mathbf{r}+\boldsymbol{\tau}) \rangle, \tag{2}$$

where $\boldsymbol{\tau}$ is the separation vector in coordinates at the location r with the first horizontal axis pointing in the local direction of the isochron, and $\langle \cdot \rangle$ denoting statistical expectation. We then expect the ACF to decay faster with increasing separation $|\boldsymbol{\tau}|$ for separation vectors $\boldsymbol{\tau}$ perpendicular to the local isochron than for $\boldsymbol{\tau}$ parallel to the isochron.

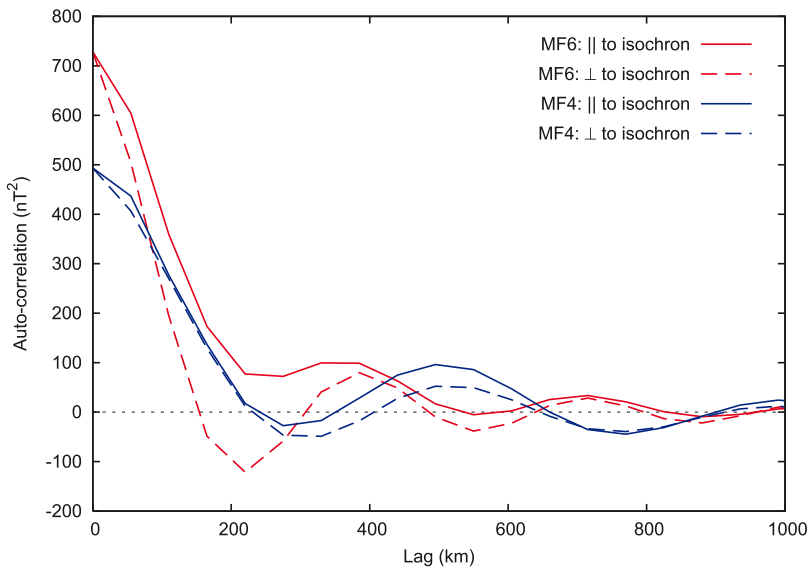

Figure 8. Autocorrelation of the vertical component of the magnetic field in ocean areas younger than 80 million years, parallel and perpendicular to the direction of the local isochron, for models MF4 and MF6. The strong anisotropy in MF6 supports our assertion that MF6 resolves the direction of magnetic lineations parallel to the isochrons of the oceanic crust.

[23] To estimate the respective ACFs, global grids of B_z with 30 arc minute resolution were generated for MF4, MF5 and MF6. Using the age grid of *Müller et al.* [2008], all oceanic grid cells younger than 80 million years were selected. For all pairs of cells with a separation of less than 1000 km (the chosen cutoff distance of the ACF), we then computed the angle between the separation vector and the average direction of the local isochron. Pairs whose separation was aligned to within 15° of the direction of the isochron were classified as "parallel," while pairs with an angle >75° to the isochron were classified as "perpendicular." All other pairs were rejected. The pairs of parallel and perpendicular autocorrelation functions are shown for MF4 and MF6 in Figure 8. With magnetic lineations trending along the isochrons, one expects the ACF to fall off more rapidly in the direction perpendicular to the isochrons. Indeed, this behavior is prevalent in the higher-resolution MF6 model, while it is hardly noticeable in the earlier, lower-resolution MF4 model. As expected, the ACFs for MF5 (not shown here) lie in between the curves for MF4 and MF6. This analysis demonstrates that the model resolution has increased sufficiently from MF4 to MF6 to resolve the age structure of the oceanic crust.

4. Conclusions and Outlook

[24] Using the latest readings of the CHAMP fluxgate magnetometer, including an improved scalar data product, we have estimated the lithospheric magnetic field to degree 120, corresponding to a 333 km wavelength resolution. The data were found to be sensitive to crustal field variations up to degree 150 (down to 266 km wavelength), but a clean separation of the lithospheric signal from ionospheric and magnetospheric noise sources could be achieved only to degree 120. The MF6 model is the first satellite-based magnetic model to globally resolve the direction of oceanic magnetic lineations, revealing the age structure of oceanic crust. Model coefficients, grids and images are available at http://geomag.org/models/MF6.html, and as a secure long-term archive at http://earthref.org/cgi-bin/erda.cgi?n=886. Requests for the new CHAMP scalar data product should be addressed directly to Hermann Lühr, since we still regard it as an intermediate product. It is planned to have all CHAMP data reprocessed and made available through the ISDC data center at GFZ by the end of 2008.

[25] Until re-entry in 2009, CHAMP is expected to continue to provide valuable magnetic measurements under solar minimum conditions at steadily decreasing altitudes, leading to increasingly accurate lithospheric field maps. Further significant advances in resolution are expected with the European Space Agency's upcoming Swarm satellite constellation mission, scheduled for launch in 2010.

Acknowledgments

[26] We thank Mike Purucker and an anonymous reviewer for helpful comments. The operational support of the CHAMP mission by the German Aerospace Center (DLR) and the financial support for the data processing by the Federal Ministry of Education and Research (BMBF) are gratefully acknowledged.

References

Arkani-Hamed, J., R. A. Langel, and M. Purucker (1994), Scalar magnetic anomaly maps of Earth derived from POGO and Magsat data, *J. Geophys. Res.*, *99*, 24,075–24,090.

Backus, G. E. (1970), Non-uniqueness of the external geomagnetic field determined by surface intensity measurements, *J. Geophys. Res.*, *75*, 6339–6341.

Cain, J. C., Z. Wang, C. Kluth, and D. R. Schmitz (1989), Derivation of a geomagnetic model to n = 63, *Geophys. J. Int.*, *97*, 431–441.

Kuvshinov, A., and N. Olsen (2005), 3-D modelling of the magnetic field due to ocean tidal flow, in *Earth Observation With CHAMP: Results From Three Years in Orbit*, edited by C. Reigber et al., pp. 359–365, Springer, Berlin.

Langel, R. A., and W. J. Hinze (1998), *The Magnetic Field of the Earth's Lithosphere—The Satellite Perspective*, Cambridge Univ. Press, Cambridge, U. K.

Lesur, V., I. Wardinski, M. Rother, and M. Mandea (2008), GRIMM: The GFZ Reference Internal Magnetic Model based on vector satellite and observatory data, *Geophys. J. Int.*, *173*, 382–394, doi:10.1111/j.1365-246X.2008.03724.x.

Maus, S., M. Rother, R. Holme, H. Lühr, N. Olsen, and V. Haak (2002), First scalar magnetic anomaly map from CHAMP satellite data indicates weak lithospheric field, *Geophys. Res. Lett.*, *29*(14), 1702, doi:10.1029/2001GL013685.

Maus, S., M. Rother, K. Hemant, C. Stolle, H. Lühr, A. Kuvshinov, and N. Olsen (2006), Earth's lithospheric magnetic field determined to spherical harmonic degree 90 from CHAMP satellite measurements, *Geophys. J. Int.*, *164*, 319–330, doi:10.1111/j.1365-246X.2005.02833.x.

Maus, S., H. Lühr, M. Rother, K. Hemant, G. Balasis, P. Ritter, and C. Stolle (2007a), Fifth-generation lithospheric magnetic field model from CHAMP satellite measurements, *Geochem. Geophys. Geosyst.*, *8*, Q05013, doi:10.1029/2006GC001521.

Maus, S., T. Sazonova, K. Hemant, J. D. Fairhead, and D. Ravat (2007b), National Geophysical Data Center candidate for the World Digital Magnetic Anomaly Map, *Geochem. Geophys. Geosyst.*, *8*, Q06017, doi:10.1029/2007GC001643.

Müller, R. D., M. Sdrolias, C. Gaina, and W. R. Roest (2008), Age, spreading rates, and spreading asymmetry of the world's ocean crust, *Geochem. Geophys. Geosyst.*, *9*, Q04006, doi:10.1029/2007GC001743.

Olsen, N., H. Lühr, T. J. Sabaka, M. Mandea, M. Rother, L. Tøffner-Clausen, and S. Choi (2006), CHAOS—A model of Earth's magnetic field derived from CHAMP, Ørsted, and SAC-C magnetic satellite data, *Geophys. J. Int.*, *166*, 67–75, doi:10.1111/j.1365-246X.2006.02959.x.

Ravat, D., R. A. Langel, M. Purucker, J. Arkani-Hamed, and D. E. Alsdorf (1995), Global vector and scalar Magsat magnetic anomaly maps, *J. Geophys. Res.*, *100*, 20,111–20,136.

Regan, R. D., J. C. Cain, and W. M. Davis (1975), A global magnetic anomaly map, *J. Geophys. Res.*, *80*, 794–802.

Ritter, P., and H. Lühr (2006), Search for magnetically quiet CHAMP polar passes and the characteristics of ionospheric currents during the dark season, *Ann. Geophys.*, *24*, 2997–3009.

Sabaka, T. J., N. Olsen, and M. E. Purucker (2004), Extending comprehensive models of the Earth's magnetic field with Ørsted and CHAMP data, *Geophys. J. Int.*, *159*, 521–547, doi:10.1111/j.1365-246X.2004.02421.x.

Stolle, C., H. Lühr, M. Rother, and G. Balasis (2006), Magnetic signatures of equatorial spread *F* as observed by the CHAMP satellite, *J. Geophys. Res.*, *111*, A02304, doi:10.1029/2005JA011184.